Graphene Oxide Membranes with Tunable Semipermeability in Organic Solvents

*Liang Huang, Yingru Li, Qinqin Zhou, Wenjing Yuan, and Gaoquan Shi**

Graphene-based membranes have a great potential for the applications in molecular sieving and gas separation because of their unique 2D structures and adjustable nanopores or nanochannels.[1–6] A defect-free monolayer graphene is impermeable to all gases and liquids.[7] Thus, extensive work has been devoted to creating nanopores in single-layer or double-layer graphene sheets by ion bombardment[4,8] or chemical etching.[9] A porous graphene membrane can act as a filter by blocking the molecules larger than its pores. Unfortunately, the fabrication of large-area defect-free graphene sheets and the generation of high-density nanopores in these membranes still remain as great challenges. Graphene oxide (GO) can be cheaply produced in a large scale by oxidation and exfoliation of graphite.[10,11] GO sheets are dispersible in water caused by the electrostatic repulsion of their ionized functional groups, especially carboxyl groups.[12,13] Vacuum filtration[14] or drop casting[15] have been used to prepare GO membranes (GOMs) with layered structures. The 2D nanochannels between adjacent GO layers can be used as 2D passages for molecules smaller than the thicknesses of the channels, while blocking the larger species.[16] Li et al. first explored the water separation performance of chemically reduced GO (rGO) membranes and found that the corrugations of rGO sheets could be tuned by hydrothermal treatment to provide passages for water and nanoparticles.[17] Recently, the molecular sieving performances of GOMs in aqueous solutions have been extensively studied.[5,15,16,18–23] The narrow channel-size distribution of GOMs provides them with better performances in precise molecular sieving than those of commonly used polymeric membranes.[21] However, GOMs are easy to disintegrate in aqueous media because of the highly hydrophilic oxygen-containing groups on GO sheets.[24] To improve their stability, GO sheets have to be cross-linked with multivalent ions or organic crosslinkers.[19,24] GO membranes have also been applied for the separtion of water from organic solvents via a pervaporation process.[25,26] However, the semipermeability of GO membranes in organic media and the permeation mechanism of organic solutes through these membranes have not yet been systematically studied.

On the other hand, chemical syntheses involved in chemical or pharmaceutical industry are frequently performed in organic media. In these systems, the products need to be separated from residual reactants, catalysts and/or by-products. Thus, separation membranes that can be operated in various organic solvents are expected. Polymeric nanofiltration membranes are mostly designed for the applications in aqueous media; they usually cannot preserve their separation performances or even disintegrate in organic solvents.[27] Several organic solvent nanofiltration (OSN) membranes have been developed for molecular sieving and purification in organic media.[27] However, an OSN membrane is operable only in few specific solvents. Thus, "multipurpose membranes" that workable in a variety of organic solvents are required. In this paper, we report that GOMs can be used for this purpose. GOMs are stable in various organic solvents and the sizes and surface properties of their nanochannels can be easily modulated by thermal annealing or solvation. Thus, the semipermeability of GOMs is tunable for molecular sieving.

GO was synthesized by a modified Hummers method.[28] The GO sheets have lateral dimensions of several micrometers and a thickness about 0.8 nm (Figure S1, Supporting Information), reflecting their monolayer structures.[13] GOMs were deposited on nylon microfiltration membranes by vacuum filtration. The thicknesses of GOMs were controlled by the volumes of the filtered GO suspensions. The surface of a GOM has wrinkles (**Figure 1**a), and its cross-section shows a typical layered structure (Figure 1b). Dry GOMs are mechanically strong and flexible. However, they were seriously swelled in water within several hours and disintegrated upon weak shaking (Figure S2, Supporting Information). This phenomenon is in agreement with previous reports[24] and it is attributed to the highly hydrophilic oxygen-containing functional groups on GO sheets. In a sharp contrast, GOMs are physically stable in various organic solvents (e.g., acetone, ethanol, toluene, and *n*-hexane) with polarities weaker than that of water. The solvent-soaked GOMs remained intact even after a violent shaking (Figure S2, Supporting Information); this property is prerequisite for their applications in organic solvents.

The experimental set used for permeation tests is schematically illustrated in Figure 1c. The thickness of GOM was optimized to be around 1 μm by considering its uniformity and permeability. In the case of using *p*-xylene as the solute and ethanol as the solvent, the feed compartment was filled with 100 mL ethanol solution of 1.0 mol L^{-1} *p*-xylene and the permeate compartment contained equal volume pure solvent. UV–vis spectroscopy was used to detect the concentration of *p*-xylene in the permeate compartment. The permeate solution showed strong absorption peaks of *p*-xylene after only 0.55 h and the signals intensified rapidly with permeation time (inset of Figure 1d). Accordingly, the amount of *p*-xylene permeated through GO membranes increased linearly with time in the first 3 h (Figure 1d). The slope of this line gives a permeation

L. Huang, Y. Li, Q. Zhou, W. Yuan, Prof. G. Shi
Country Collaborative Innovation Center for Nanomaterial Science and Engineering
Department of Chemistry
Tsinghua University
Beijing 100084, P. R. China
E-mail: gshi@tsinghua.edu.cn

DOI: 10.1002/adma.201500975

ADVANCED MATERIALS
www.advmat.de

www.MaterialsViews.com

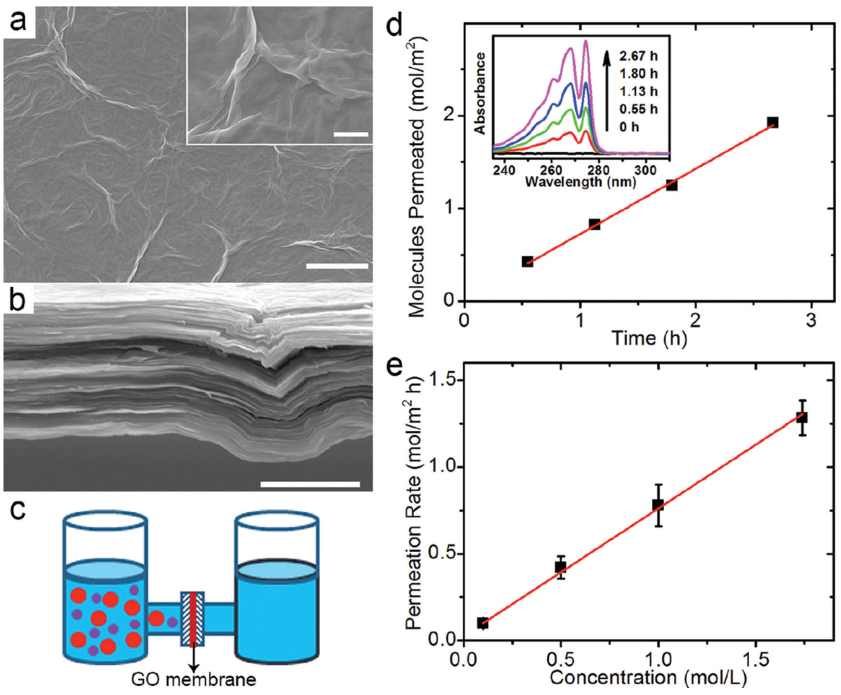

Figure 1. The morphology of a GOM and the permeation of *p*-xylene through a 1 μm thick GOM in ethanol. a) Top-view SEM image of a GOM, the scale bar is 100 μm; the inset is a magnified view of wrinkles, the scale bar is 10 μm. b) Cross-sectional SEM image of a GOM, the scale bar is 10 μm. c) Schematic illustration of the experimental set used for permeation tests. d) Permeation of 1.0 mol L^{-1} *p*-xylene; inset shows the UV–vis spectra of the permeate solution at different time. e) Permeation rates as a function of the *p*-xylene concentration in the feed solution.

rate of 0.78 mol m^{-2} h^{-1} for 1.0 mol L^{-1} *p*-xylene. The permeation rate of *p*-xylene has a linear relationship with its concentration in the feed solution (Figure 1e).

To systematically investigate the semipermeability of GOM, we chose a series of molecules with different sizes as solutes (Figure S3, Supporting Information). The permeation rates of these solute molecules in ethanol are summarized in **Figure 2**.

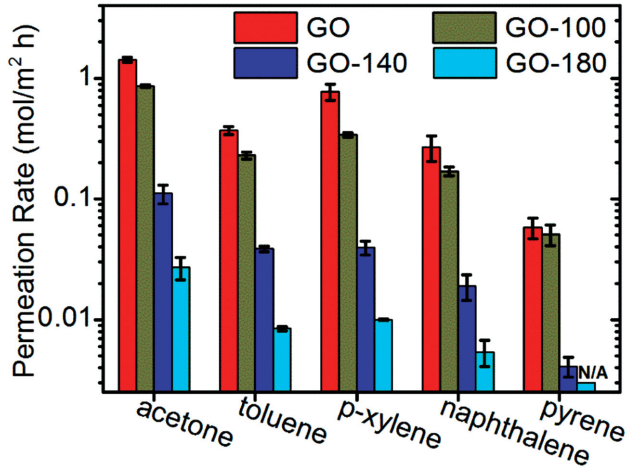

Figure 2. Permeation rates of different solute molecules through a 1 μm thick GOM in ethanol. The permeation rates are normalized to those of 1.0 mol L^{-1} feed solutions; N/A means not available.

Accordingly, the permeation rate decreases with the increase in the size of solute molecules. For example, acetone showed the highest permeation rate of 1.43 ± 0.07 mol m^{-2} h^{-1} because of its smallest molecular size among the tested molecules. This value is about 25 times higher than that of pyrene (0.058 ± 0.011 mol m^{-2} h^{-1}). If the molecules are sufficiently large (e.g., Lumogen Red 300), no molecule permeation was detected even after 1 week of permeation time (Figure S4, Supporting Information). It is interesting to note that the permeation rate of toluene is lower than that of *p*-xylene, while the former has a smaller molecular size.

The semipermeability of GOMs can be tuned by thermal annealing. For this purpose, GOMs were thermally annealed at 100 or 140 °C for 2 h or at 180 °C for 1.5 h. They were nominated as GO-100, GO-140, or GO-180, respectively. As shown in Figure 2, the increase of annealing temperature decreased the permeability of GOM. Taking *p*-xylene as an example, its permeation rate in ethanol through GO-100 was measured to be 0.34 ± 0.01 mol m^{-2} h^{-1}, while that for GO-140 decreased to 0.040 ± 0.005 mol m^{-2} h^{-1}. Particularly, pyrene molecules were completely blocked by GO-180 membrane.

Thermal annealing narrowed the nanochannels and reduced the oxygen-containing groups of GOMs, leading to the decrease of their permeability. The d-spacing of a dry GOM was measured to be 0.83 nm by X-ray diffraction (XRD, **Figure 3**a). After annealing, the diffraction peak of GOMs shifted to higher angles, suggesting the reduction of d-spacing (Figure 3b); higher annealing temperature led to forming smaller d-spacing. For example, GO-180 exhibited a d-spacing of 0.61 nm, while that of GO-140 was measured to be 0.68 nm. The d-spacings of these annealed GOMs were expanded upon soaking in ethanol (Figure 3). The d-spacing of ethanol-soaked GO-180 membrane was expanded to 1.32 nm, and this value is smaller than that of ethanol-swelled GOM (1.58 nm).

The structural evolution of GOM upon annealing at different temperatures was monitored by X-ray photoelectron spectroscopy (XPS). The C1s XPS spectrum of a GOM or an annealed GOM can be divided into four peaks (**Figure 4**a), corresponding to four types of carbon bonds: CC/C=C (284.6 eV), COH/COC (286.6 eV), C=O (287.7 eV), and HOC=O (289.0 eV).[29] Hereinafter, the percentages of CC/C=C or COH/COC peak area in the C1s spectrum are designated as P_C or P_{CO}. P_C slightly increased and P_{CO} concurrently decreased with the increase of annealing temperature (Figure 4b), implying the loss of oxygen-containing groups. This conclusion has been further confirmed by the increase of C/O atomic ratio (Figure 4b). The loss of oxygen-containing groups is responsible for the narrowing of d-spacing of GOM upon annealing. The Raman spectra of pristine and annealed GOMs showed D- and G-bands of graphene,

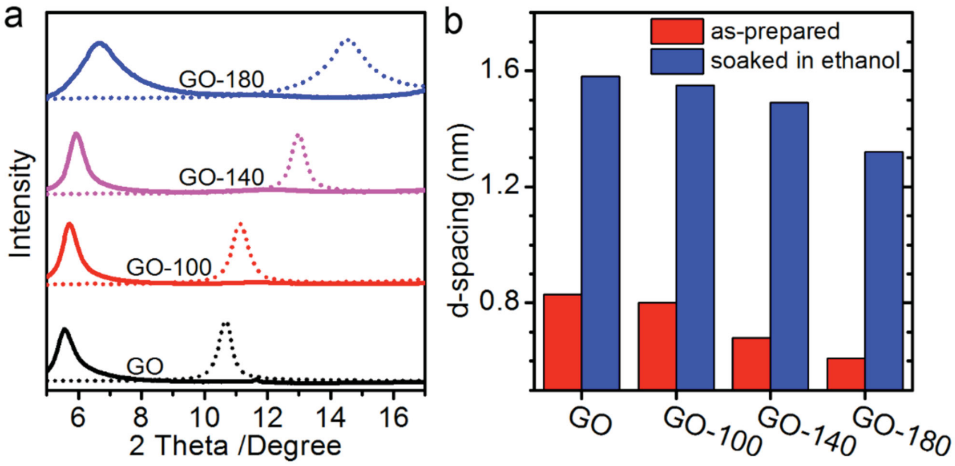

Figure 3. The structural changes of GOMs before and after soaking in ethanol. a) XRD patterns of as-prepared (dashed line) and ethanol-soaked GOMs (solid line). b) The d-spacings of GOMs before and after soaking in ethanol.

and annealing did not change the intensity ratio of both bands (Figure 4c). This observation is in accordance with that reported in literature and suggests that the sizes of sp^2 clusters in graphene sheets were unchanged.[30] However, the areal percentage of sp^2 regions in GO sheet should be increased upon annealing by considering the increases in P_C and C/O atomic ratio. Pyrene molecules have strong π–π interaction with the sp^2 regions of GO; thus, the permeation rate of pyrene decreased rapidly with the increase of annealing temperature. Finally, they were entirely blocked by GO-180 membrane.

The semipermeability of GOMs can also be modulated by solvation. A GOM can be swelled by organic solvents and the degrees of solvation depend on the properties of the solvents.[31] By carefully choosing solvents, the nanochannel sizes of GOMs can be regularly modulated (**Figure 5** and Figure S5a, Supporting Information). For example, the d-spacings of a dry GOM and the GOMs soaked in ethanol, acetone, toluene, and *n*-hexane were measured by XRD to be 0.83, 1.58, 1.29, 0.84, and 0.88 nm, respectively. GOMs were reported to be not swelling in nonpolar solvents,[31] their slight expansion by toluene or *n*-hexane in our system is possibly attributed to the trace water in solvent or from air. Interestingly, the d-spacing of a GOM can also be tuned by using mixtures of organic solvents (Figure S5b, Supporting Information). The permeability of a GOM decreased with the decrease of its d-spacing in solvent. The permeation rate of pyrene through acetone solvated GOM was lower than that through the ethanol solvated counterpart (Figure 5b). The toluene or *n*-hexane solvated GOMs totally blocked pyrene molecules.

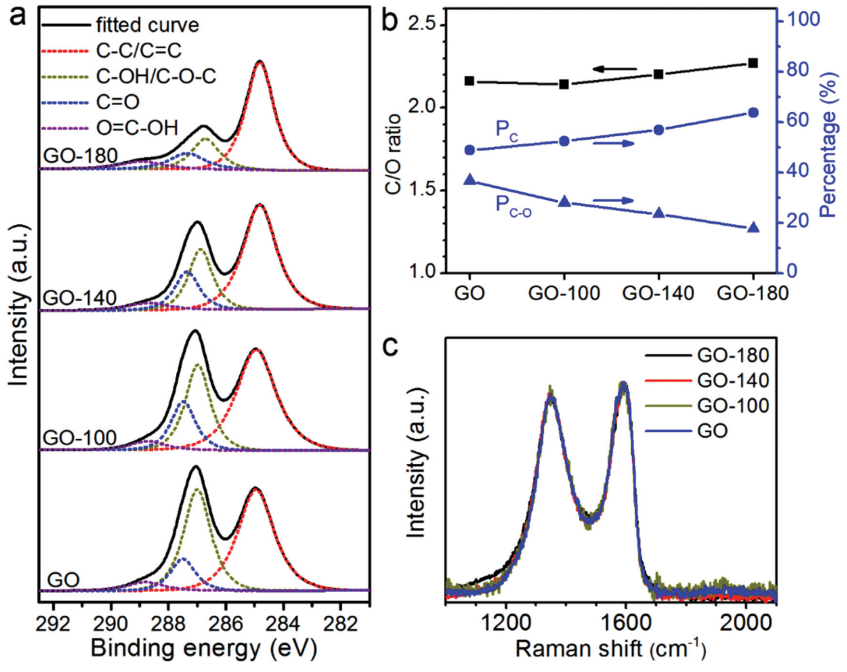

Figure 4. The structural evolution of GOMs during thermal annealing. a) C1s XPS spectra of GOMs annealed at different temperatures. b) The changes of C/O atomic ratio, P_C and P_{CO} with annealing temperature. c) Raman spectra of GO membranes annealed at different temperatures.

Dialysis is a common laboratory technique, especially in biochemistry lab. Dialysis membranes are typically made of regenerated cellulose or cellulose esters. Although they show good performances in aqueous media, their poor resistance to common organic solvents such as ethanol and acetone strongly limit their practical applications. Since GOMs showed good molecular sieving performances in organic solvents, here we explored their possible applications in dialysis. As a demonstration, toluene and Lumogen Red 300 were chosen as models of small and big molecules. The feed compartment was loaded with a mixed ethanol solution of toluene (1.0 mol L^{-1}) and Lumogen Red 300 (0.2 μmol L^{-1}), and the permeate compartment was filled with pure ethanol. Toluene and Lumogen Red 300 have optical absorptions at different spectral regions;

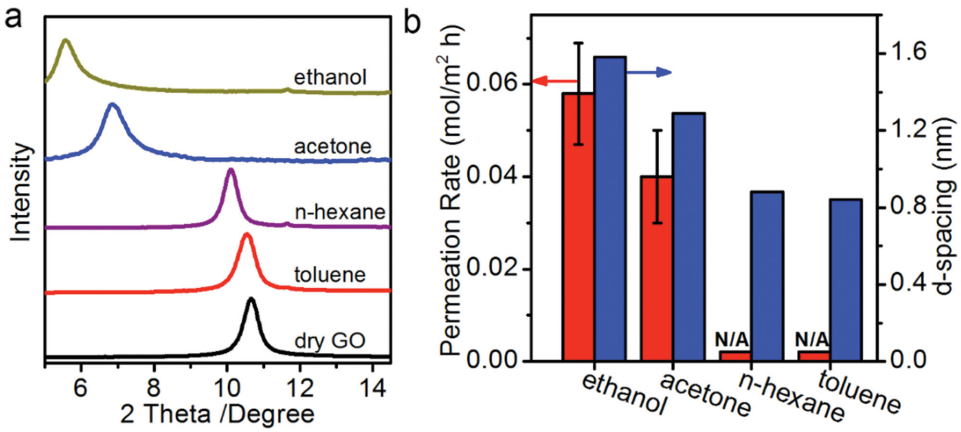

Figure 5. Tuning the permeation rate of pyrene through a 1 μm thick GOM by using different solvents. a) XRD patterns of dry and solvent-soaked GOMs. b) The d-spacings of solvent-soaked GOMs and the permeation rates of pyrene in different solvents.

thus their concentrations in the permeate compartment can be monitored simultaneously. We did not detect any absorption of Lumogen Red 300 in the permeate compartment within 2 weeks. However, the percentage of toluene molecules retained in the feed compartment decreased linearly with time within 91 h (Figure S6, Supporting Information). This result implied that the addition of Lumogen Red 300 did not block the nanochannels of GOM, while it was totally rejected by the membrane. Therefore, GOM is a promising material for the dialysis in organic solvents.

A model has been proposed by Geim et al. to explain the unimpeded evaporation of water through GOMs.[1] In this model, a GO sheet was divided into two types of regions: oxidized and pristine. The oxidized regions act as spacers to keep adjacent GO sheets apart and help water molecules to intercalate between GO sheets. The pristine regions provide a network of capillaries that allow nearly frictionless flow of water. However, GO is known as an insulator.[32,33] Thus, the pristine regions are unlikely to form a continuous network across a GO sheet. On the other hand, ultra-high-resolution transmission electron microscopy studies indicate that an as-synthesized GO sheet consists of three types of regions: holes, pristine graphitic, and oxidized regions with areal percentages of approximately 2%, 16%, and 82%, respectively.[34–36] The oxidized regions form a continuous network across a GO sheet with pristine regions as isolated islands. This model explains why GO has an extremely low conductivity. The isolated pristine regions were also confirmed by Raman spectroscopic studies.[30]

As described above, the average areal percentage of holes in a GO sheet is as small as 2%; thus these pores will be tightly blocked by the impermeable oxidized and pristine regions of adjacent GO sheets during the formation of a membrane. A GOM with a thickness of 1 μm should have over one thousand layers of GO sheets; consequently, the contribution of physical holes to the permeability of GOM is negligible. We assume that the oxidized regions of adjacent GO sheets in a GOM were assembled mainly in a face-to-face mode. This assumption is reasonable as considering the strong interaction between oxygen-containing groups and the continuous network of oxidized regions in individual GO sheet. An anhydrous GOM was reported to have a d-spacing of about 0.60 nm,[37] corresponding to the thickness of oxidized regions. Taking account of the thickness of a pristine graphene sheet (0.34 nm), each pristine region in GOM should have a void space of about 0.26 nm. These void spaces are separated by the surrounding oxidized regions. Because GO is highly hydrophilic, one or two layers of water molecules will be adsorbed on the surfaces of GO channels in air, depending on the humidity of environment. At a relative humidity of about 40%, the as-prepared GOM exhibited an XRD peak at $2\theta = 10.67°$ (Figure 3a), corresponding to a d-spacing of 0.83 nm.[37] For GO membranes soaked in ethanol, the XRD peak was shifted to $2\theta = 5.7°$ (d-spacing = 1.58 nm). XRD peak of GOM in ethanol was not broadened notably comparing with that of a dry GOM. This result reflects that the layered structure of GOM was preserved and a solvent layer with a uniform thickness of about 0.98 nm was intercalated between adjacent GO layers. This intercalated solvent layer is large enough to accommodate pyrene molecules (0.92 nm × 0.69 nm × 0.34 nm) to allow them permeate through GOMs. In contrast, large molecules like Lumogen Red 300 (2.2 nm × 1.6 nm × 1.0 nm) are too large to diffuse into the intercalated solvent layer; thus they were blocked.

The effective diffusivity of a solute within a pore with comparable size is frequently found to be smaller than that in a bulk solution.[38] This phenomenon is known as hindered or restricted diffusion mainly caused by pore walls. When the size of solute is close to that of pores, the collisions between solute molecules and pore walls significantly hinder the diffusion of solute molecules. The hindered diffusion of an uncharged spherical solute in straight through cylindrical pores can be estimated by Renkin equation:[39]

$$D_m/D_o = (1-\lambda)^2(1-2.104\lambda+2.09\lambda^3-0.95\lambda^5)$$

where D_m/D_o is the ratio of solute diffusion coefficient in the pore to that in solution and λ is the diameter ratio of solute and pore (d_s/d_p). D_o is a constant as the solute and solvent are defined and its value can be estimated by Wilke–Chang equation (see the Supporting Information for detail).[40] Accordingly, D_m is a monotone decreasing function of λ following Renkin equation. Fick's first law[41] also indicates that the permeation rate at a given concentration gradient is proportional

to diffusion coefficient; thus, it also decreases monotonously with the increase of λ. As a result, solute with smaller diameter should have a larger permeation rate. For a GOM immersed in ethanol, its pore diameter equals to the free space between oxidized regions of adjacent GO sheets. According to Renkin equation, the permeation rate of acetone should be four times that of toluene and 18 times that of pyrene, and these theoretical results are comparable to our measured values (3.8 times for toluene and 25 times for pyrene). However, we also found that *p*-xylene exhibited a higher permeation rate than that of toluene. Renkin equation assumes solute molecules are uncharged spheres and considers only the collisions between solute molecules and pore walls. The two methyl groups in *p*-xylene might sterically hinder the π–π interaction between this aromatic molecule and the pristine regions of GO sheet. As a result, *p*-xylene molecules may encounter less resistance during diffusion. To verify this assumption, pyridine was used as a solute for comparison. Pyridine has a smaller size and much stronger interaction with GO than those of toluene.[42,43] The permeation rate of pyridine (0.084 ± 0.003 mol m^{-2} h^{-1}) was tested to be much smaller than that of toluene (0.37 ± 0.03 mol m^{-2} h^{-1}). Therefore, it is reasonable to conclude that the molecule size of solute is not the only parameter that determines its permeation rate, the interaction between solute and GO sheet is also a nonignorable factor.

In summary, GOMs are mechanically stable in various organic solvents, making them applicable for molecular sieving in organic media. In ethanol, the nanochannels of a GOM have a size of 0.98 nm; thus, small molecules such as toluene, acetone, and pyrene can permeate through it, while big molecules like Lumogen Red 300 are blocked. Furthermore, the semipermeability of GOMs can be easily engineered by thermal annealing or changing solvents, and the nanochannels of GOMs cannot be blocked by big molecules. Therefore, GOMs are promising for applications in "multipurpose membranes" for molecular sieving in various organic solvents.

Experimental Section

Preparation of GO Dispersion: GO was prepared from natural graphite powder by a modified Hummers method.[28] The product was filtered and washed with diluted HCl solution to remove metal ions followed by washing with distilled water to remove the acid. The resulting solid was dried in air and dissolved in distilled water to form a dispersion. Successively, it was purified by dialysis for 1 week to remove the remaining metal species. Finally, it was centrifuged at 4000 rpm to remove the unoxidized or uncompletely oxidized graphite powder.

Fabrication of GOMs: GOMs were fabricated by vacuum filtration of GO suspensions through nylon microfiltration membranes with a pore size of 0.22 μm. After the filtration, GO membrane was dried in air at room temperature before further treatment or installing in the testing system. The thicknesses of the membranes were controlled by the volumes of the filtered solutions. The GOMs were kept on the surfaces of nylon membranes for permeation tests because the latter provided GOMs with valuable mechanical supports. These porous supports did not show any influence on the permeability of GOMs.

Thermal Annealing of GOMs: GOMs were put in an oven and annealed at 100 or 140 °C for 2 h, or at 180 °C for 1.5 h. The relative humidity in the oven was kept to be 100% by putting in a beaker of distilled water. The high humidity prevented the cracking of GOMs during annealing. After annealing, GOMs were cooled in air and kept under ambient condition.

Permeation Tests: The permeation tests were performed using an H-shaped device as shown in Figure 1c. A photograph of our device is given in Figure S7 (Supporting Information). It consists of two tubular compartments separated by a GOM with an effective area of 2.0 cm^2. The joints between the glass compartments and GOM were sealed with perfect vacuum silicon fat and fixed with a clamp to prevent the leakage of solutions. In a typical experiment, one compartment (referred to as permeate) was filled with a solvent and kept undisturbed for about 30 min to fully wet the GOM. Actually, in the case of using ethanol, the wetting process required only several minutes (Figure S8, Supporting Information). Then the other compartment (referred to as feed) was filled with the same volume of the solution of certain solute. We used magnetic stirring in both feed and permeate compartments to avoid possible concentration gradients near the membrane. During the test, each compartment was capped with a lid to prevent the evaporation of organic solvent. Small amounts of the solution in permeate compartment were taken out at fixed time intervals for measuring the concentrations of solute.

Characterization: Scanning electron micrographs (SEM) were taken out using a Sirion-200 scanning electron microscope (FEI, USA). UV–vis spectra were carried out on a U-3010 spectrophotometer (Hitachi, Japan). Atomic force microscope (AFM) images were recorded on a SPM 9600 microscope (Shimadzu, Japan). The samples for AFM tests were prepared by drop drying diluted solutions on freshly cleaved mica sheets. XRD was performed on a D8 Advance X-ray diffractometer with Cu Kα radiation ($\lambda = 0.15418$ nm, Bruker, Germany). The XRD patterns of solvent-soaked GO membranes were collected by using a home-made sample holder (Figure S9, Supporting Information). Raman spectra were obtained by the use of a LabRAM HR Evolution (HORIBA Jobin Yvon, France) Raman microscope with a 514-nm laser. XPS spectra were taken out by using an ESCALAB 250XI photoelectron spectrometer (ThermoFisher Scientific, USA).

Supporting Information

Supporting Information is available from the Wiley Online Library or from the author.

Acknowledgements

This work was supported by the National Basic Research Program of China (2012CB933402 and 2013CB933001) and the Natural Science Foundation of China (51433005).

Received: February 26, 2015
Revised: April 10, 2015
Published online: May 20, 2015

[1] R. R. Nair, H. A. Wu, P. N. Jayaram, I. V. Grigorieva, A. K. Geim, *Science* **2012**, *335*, 442.
[2] H. W. Kim, H. W. Yoon, S. M. Yoon, B. M. Yoo, B. K. Ahn, Y. H. Cho, H. J. Shin, H. Yang, U. Paik, S. Kwon, J. Y. Choi, H. B. Park, *Science* **2013**, *342*, 91.
[3] H. Li, Z. Song, X. Zhang, Y. Huang, S. Li, Y. Mao, H. J. Ploehn, Y. Bao, M. Yu, *Science* **2013**, *342*, 95.
[4] K. Celebi, J. Buchheim, R. M. Wyss, A. Droudian, P. Gasser, I. Shorubalko, J. I. Kye, C. Lee, H. G. Park, *Science* **2014**, *344*, 289.
[5] R. K. Joshi, P. Carbone, F. C. Wang, V. G. Kravets, Y. Su, I. V. Grigorieva, H. A. Wu, A. K. Geim, R. R. Nair, *Science* **2014**, *343*, 752.
[6] S. C. O'Hern, C. A. Stewart, M. S. H. Boutilier, J.-C. Idrobo, S. Bhaviripudi, S. K. Das, J. Kong, T. Laoui, M. Atieh, R. Karnik, *ACS Nano* **2012**, *6*, 10130.

ADVANCED MATERIALS
www.advmat.de

Materials Views
www.MaterialsViews.com

[7] J. S. Bunch, S. S. Verbridge, J. S. Alden, Arend M. van der Zande, J. M. Parpia, H. G. Craighead, P. L. McEuen, *Nano Lett.* **2008**, *8*, 2458.
[8] S. C. O'Hern, M. S. H. Boutilier, J.-C. Idrobo, Y. Song, J. Kong, T. Laoui, M. Atieh, R. Karnik, *Nano Lett.* **2014**, *14*, 1234.
[9] S. P. Koenig, L. Wang, J. Pellegrino, J. S. Bunch, *Nat. Nanotechnol.* **2012**, *7*, 728.
[10] S. Park, R. S. Ruoff, *Nat. Nanotechnol.* **2009**, *4*, 217.
[11] M. Segal, *Nat. Nanotechnol.* **2009**, *4*, 611.
[12] D. Li, M. B. Müller, S. Gilje, R. B. Kaner, G. G. Wallace, *Nat. Nanotechnol.* **2008**, *3*, 101.
[13] H. Bai, C. Li, X. Wang, G. Shi, *J. Phys. Chem. C* **2011**, *115*, 5545.
[14] D. A. Dikin, S. Stankovich, E. J. Zimney, R. D. Piner, G. H. Dommett, G. Evmenenko, S. T. Nguyen, R. S. Ruoff, *Nature* **2007**, *448*, 457.
[15] P. Sun, M. Zhu, K. Wang, M. Zhong, J. Wei, D. Wu, Z. Xu, H. Zhu, *ACS Nano* **2012**, *7*, 428.
[16] H. Huang, Y. Ying, X. Peng, *J. Mater. Chem. A* **2014**, *2*, 13772.
[17] L. Qiu, X. Zhang, W. Yang, Y. Wang, G. P. Simon, D. Li, *Chem. Commun.* **2011**, *47*, 5810.
[18] Y. Han, Z. Xu, C. Gao, *Adv. Funct. Mater.* **2013**, *23*, 3693.
[19] M. Hu, B. Mi, *Environ. Sci. Technol.* **2013**, *47*, 3715.
[20] H. Huang, Z. Song, N. Wei, L. Shi, Y. Mao, Y. Ying, L. Sun, Z. Xu, X. Peng, *Nat. Commun.* **2013**, *4*, 2979.
[21] B. Mi, *Science* **2014**, *343*, 740.
[22] H. Huang, Y. Mao, Y. Ying, Y. Liu, L. Sun, X. Peng, *Chem. Commun.* **2013**, *49*, 5963.
[23] P. Sun, F. Zheng, M. Zhu, Z. Song, K. Wang, M. Zhong, D. Wu, R. Little, Z. Xu, H. Zhu, *ACS Nano* **2014**, *8*, 850.
[24] C.-N. Yeh, K. Raidongia, J. Shao, Q.-H. Yang, J. Huang, *Nat. Chem.* **2015**, *7*, 166.
[25] R. Liu, G. Arabale, J. Kim, K. Sun, Y. Lee, C. Ryu, C. Lee, *Carbon* **2014**, *77*, 933.
[26] K. Huang, G. Liu, Y. Lou, Z. Dong, J. Shen, W. Jin, *Angew. Chem. Int. Ed.* **2014**, *53*, 6929.
[27] P. Marchetti, M. F. Jimenez Solomon, G. Szekely, A. G. Livingston, *Chem. Rev.* **2014**, *21*, 10735.
[28] J. William, S. Hummers, R. E. Offeman, *J. Am. Chem. Soc.* **1958**, *80*, 1339.
[29] D. Yang, A. Velamakanni, G. Bozoklu, S. Park, M. Stoller, R. D. Piner, S. Stankovich, I. Jung, D. A. Field, C. A. Ventrice, R. S. Ruoff, *Carbon* **2009**, *47*, 145.
[30] C. Mattevi, G. Eda, S. Agnoli, S. Miller, K. A. Mkhoyan, O. Celik, D. Mastrogiovanni, G. Granozzi, E. Garfunkel, M. Chhowalla, *Adv. Funct. Mater.* **2009**, *19*, 2577.
[31] K. W. Putz, O. C. Compton, C. Segar, Z. An, S. T. Nguyen, L. C. Brinson, *ACS Nano* **2011**, *5*, 6601.
[32] Q. Zhang, H. Zheng, Z. Geng, S. Jiang, J. Ge, K. Fan, S. Duan, Y. Chen, X. Wang, Y. Luo, *J. Am. Chem. Soc.* **2013**, *135*, 12468.
[33] K. Hatakeyama, H. Tateishi, T. Taniguchi, M. Koinuma, T. Kida, S. Hayami, H. Yokoi, Y. Matsumoto, *Chem. Mater.* **2014**, *26*, 5598.
[34] K. Erickson, R. Erni, Z. Lee, N. Alem, W. Gannett, A. Zettl, *Adv. Mater.* **2010**, *22*, 4467.
[35] D. Pacilé, J. C. Meyer, A. Fraile Rodríguez, M. Papagno, C. Gómez-Navarro, R. S. Sundaram, M. Burghard, K. Kern, C. Carbone, U. Kaiser, *Carbon* **2011**, *49*, 966.
[36] C. Gomez-Navarro, J. C. Meyer, R. S. Sundaram, A. Chuvilin, S. Kurasch, M. Burghard, K. Kern, U. Kaiser, *Nano Lett.* **2010**, *10*, 1144.
[37] A. Lerf, A. Buchsteiner, J. Pieper, S. Schottl, I. Dekany, T. Szabo, H. P. Boehm, *J. Phys. Chem. Solids* **2006**, *67*, 1106.
[38] M. P. Bohrer, G. D. Patterson, P. J. Carroll, *Macromolecules* **1984**, *17*, 1170.
[39] E. M. Renkin, *J. Gen. Physiol.* **1956**, *39*, 820.
[40] K. Miyabe, R. Isogai, *J. Chromatogr. A* **2011**, *1218*, 6639.
[41] S. T. Cui, *J. Chem. Phys.* **2005**, *123*, 054706.
[42] J. I. Paredes, S. Villar-Rodil, A. Martínez-Alonso, J. M. D. Tascón, *Langmuir* **2008**, *24*, 10560.
[43] Z. Tang, X. Wu, B. Guo, L. Zhang, D. Jia, *J. Mater. Chem.* **2012**, *22*, 7492.